analytical chemistry

Article

pubs.acs.org/ac

Exploiting Surface-Plasmon-Enhanced Light Scattering for the Design of Ultrasensitive Biosensing Modality

Chih-Tsung Yang,[†] Lin Wu,[§] Xiaohu Liu,[‡] Nhung Thi Tran,[‡] Ping Bai,[§] Bo Liedberg,[*,‡] Yi Wang,[*,‡,∥,⊥] and Benjamin Thierry[*,†]

[†]Future Industries Institute, University of South Australia, Mawson Lakes Campus, Mawson Lakes, South Australia 5095, Australia

[‡]Center for Biomimetic Sensor Science, School of Materials Science and Engineering, Nanyang Technological University, Singapore 639798

[§]Electronics and Photonics Department, Institute of High Performance Computing, Agency for Science, Technology, and Research (A*STAR), Singapore 138632

[∥]Wenzhou Institute of Biomaterials and Engineering, Chinese Academy of Sciences, Wenzhou, Zhejiang 325001, China

[⊥]Institute of Biomaterials and Engineering, Wenzhou Medical University, Wenzhou, Zhejiang 325035, China

Supporting Information

ABSTRACT: Development of new detection methodologies and amplification schemes is indispensable for plasmonic biosensors to improve the sensitivity for the detection of trace amounts of analytes. Herein, an ultrasensitive scheme for signal enhancement based on the concept of surface-plasmon-resonance-enhanced light scattering (SP-LS) was validated experimentally and theoretically. The SP-LS of gold nanoparticles' (AuNPs) tags was employed in a sandwich assay for the detection of cardiac troponin I and provided up to 2 orders of magnitude improved sensitivity over conventional AuNPs-enhanced refractometric measurements and 3 orders of magnitude improvement over label-free SPR. Simulations were also performed to provide insights into the physical mechanisms.

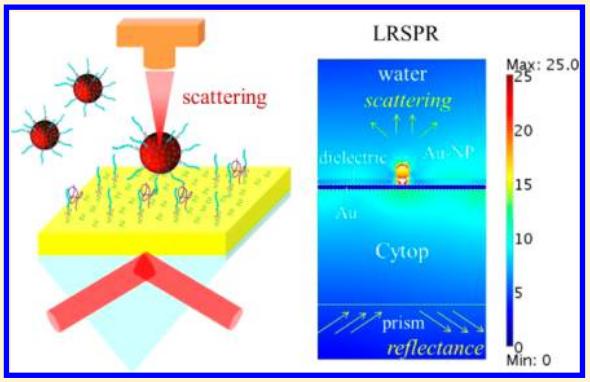

Plasmonics, the science of surface plasmons propagating at the metal/dielectric interfaces or localized to nanoscale objects, is a major technological innovation which has found significant applications in numerous fields. With respect to immunoassaying, surface plasmon resonance (SPR) is among the most efficient and versatile solid-state biosensing technologies. The development of advanced detection methodologies and amplification schemes has significant scope to further increase the biomedical significance of plasmonic biosensors.[1−4] A range of signal amplification approaches based on the "sandwich immunoassay" principle have been implemented for the improvement of SPR sensitivity and specificity. These include assays based on enzymatic reactions,[5−7] nanoparticle amplification,[8,9] and surface-plasmon-enhanced fluorescence spectroscopy (SP-FS).[10,11] SP-FS provides exquisite sensitivity for the detection of biomarkers; however, fluorescence can be quenched when the fluorescent tag is too close to the sensor surface (<10 nm), which requires careful experimental design.

In addition, SP-FS is susceptible to photobleaching. Metallic nanoparticle amplification tags are an excellent alternative because of their optical characteristics and ease of functionalization.[12,13] Localized surface plasmon resonance waves (LSPR) associated with noble metal nanoparticles, including gold nanoparticles (AuNPs), couple with surface plasmon waves on the planar metal film[14] and in turn efficiently boost enhancement and sensitivity of SPR biosensors in the reflectivity mode.[9] However, AuNPs-enhanced refractometric measurements mainly reflect the effects of the SPR, as LSPR are only measured indirectly, which results in only limited sensitivity improvement. Most studies to date have focused on the optimization of AuNP sizes and shapes, yielding only moderate signal enhancement.[15−19] Toward improving the sensitivity of SPR immunoassays, gold nanorods have been employed as amplification tags for the tumor necrosis factor alpha antigen in a phase interrogation scheme.[20] A 40-fold increased sensitivity was obtained as compared with label-free refractometric SPR, demonstrating the significance of advanced detection schemes.

We report here an ultrasensitive assay concept based on the principle of surface-plasmon-enhanced light scattering (SP-LS), in which the scattering from AuNPs secondary molecular probes is measured directly. We hypothesized that if the large localized electromagnetic field associated with the excitation of plasmonic metal particles by surface plasmons could be

Received: September 26, 2016
Accepted: November 8, 2016
Published: November 8, 2016

DOI: 10.1021/acs.analchem.6b03798
Anal. Chem. 2016, 88, 11924−11930

measured directly, the advantages of the nanoparticle secondary probes could be fully exploited. The proof-of-concept is demonstrated experimentally using cardiac troponin-I (cTnI) used here as a model biomarker. These experimental measurements revealed that the SP-LS of AuNPs provides up to 2 orders of magnitude improved sensitivity over conventional AuNPs-enhanced refractometric SPR measurements and 3 orders of magnitude improvement over label-free SPR measurements. Theoretical simulation of the SP-LS sensing scheme confirmed that its improved sensitivity is linked to the strong electromagnetic field enhancement of the AuNPs, which translates into very high scattering signals even at low analyte concentration. The inherent abilities of AuNPs to strongly scatter light upon the excitation of their surface plasmon oscillation has been long recognized and exploited for the design of colorimetric assays and in the molecular imaging field as an alternative to fluorescence-based approaches.[21,22] A hydrodynamic model was previously built up to describe the AuNPs scattering behavior based on dark-field microscopy.[23] In addition, the early study by Jory et al. demonstrated the possibility of detecting the scattering of latex particles excited by SPs.[24] Recently, the evanescent light scattering has been employed to visualize single surface-bound lipid vesicles without the fluorescent dye labeling.[25] The proposed concept of SP-LS assay builds on these concepts toward the development of an ultrasensitive biosensing scheme, and the excellent sensitivity obtained supports its applications in molecular biosensing, especially for the detection of low-molecular-weight biomarkers found at low concentration.

EXPERIMENTAL SECTION

Materials. The peptide binder TP (CALNN-Peg4-FYSHSFHENWPS) and peptide spacer (CALNN) were customized and purchased from GL, Shanghai. Human cardiac troponin I (cTnI) was obtained from Abcam, U.S. $HAuCl_4 \cdot 3H_2O$, sodium citrate, hydroquinone, and Tween-20 were purchased from Sigma-Aldrich. Phosphate-buffered saline acquired from Sigma-Aldrich was used to prepare 10 mM phosphate buffer. PBST buffer was prepared by dissolving 0.05% of Tween-20 in phosphate buffer.

Synthesis of AuNPs. The 36 nm in diameter sized gold nanoparticles were synthesized with slight modification of the standard citrate reduction method.[26] Briefly, 100 mL of 0.01% (0.1 mg/mL) gold(III) chloride trihydrate solution was boiled in a well-cleaned flask. After the mixture was boiled, 1.75 mL of 1% (10 mg/mL) sodium citrate was added into the flask in order to obtain 36 nm AuNPs. It was then kept boiling until the color changed from light yellow to red. The synthesized spherical gold nanoparticles were verified by DLS (Figure S1a) and TEM (Figure S1b), and the nanoparticles were stored in the fridge until use.

Preparation of Sensor Chips. The SPR-supported chips were glass substrates coated with ∼2 nm Cr and ∼47 nm Au film, whereas the LRSPR chips consisted of a low refractive index layer (i.e., ∼ 750 nm of Cytop) coated with ∼17 nm Au film.[27]

Preparation of TP-Functionalized Gold Film and AuNPs. Gold substrates were functionalized with TP and CALNN (1:1 molar ratio, 1 mM in water) by incubating the cleaned bare gold substrates with the peptide mixture overnight. The substrates were rinsed with water and mounted in the SPR instrument. For the modification of TP on AuNPs, the peptide spacer CALNN (12.5 μL, 2 mM) and TP (25 μL, 1 mM) were mixed in 500 μL of phosphate-buffered saline buffer (1× , 0.05% Tween). This solution was then mixed with 1 mL of AuNPs and left to react overnight. The biofunctionalized AuNPs were purified by triple centrifugations, and the successful modification was monitored by UV−vis spectroscopy (Figure S1c). TP-functionalized AuNPs were stored at 4 °C until use.

Optical Setup. The SPR system and its operation software Wasplas were developed at the Max Planck Institute of Polymer Research (Germany). Briefly, the setup for the light scattering measurement was discussed in detail as described previously.[11] The scattering light emitted from the sensor surface was collected through the flow-cell by a lens (numerical aperture NA = 0.3), passed through a ND filter, and its intensity was detected by a photomultiplier tube (PMT). The flow-cell made of PDMS spacer with a volume of 10 μL was pressed against the sensor surface and a quartz lid connected with the tubing (inner diameter = 0.13 mm, Tygon R3607) through the inlet and outlet for sample circulation. The peristaltic pump was used to pump samples into the flow-cell for measurement at the flow rate of 50 μL/min.

Simulations. In the simulation, three-dimensional Maxwell's equations were solved using the finite element method (COMSOL Multiphysics). At a fixed incident light wavelength (λ_0 = 632.8 nm), the dielectric function of gold was taken as $0.18 + 3.5i$ (or $0.21 + 3.29i$) for the 47 nm-thick (or 17 nm-thick) gold film, and $0.6 + 2.25i$ for the gold nanoparticles (AuNPs); the dielectric function of chromium was taken as $3.14 + 3.31i$. The refractive indices for water, Cytop, the prism LaSFN9, and the peptide layer were 1.333, 1.337, 1.845, and 1.45, respectively.

A unit cell consisting of one nanoparticle sitting on a multilayered SPR or LRSPR substrate was simulated by setting its lateral dimension as the pitch, p, which defines the center-to-center distance between nanoparticles. At the sides of the unit cell, Floquet periodic boundary condition was assumed in order to obtain the optical response of the whole array to a light source illuminating from an angle. At the top and bottom of the unit cell, we set a water perfectly matched-layer (PML) and a LaSFN9 PML to mimic the open boundaries (i.e., strongly absorb outgoing waves from the interior of a computational region without reflecting them back into the interior).

An obliquely incident TM-polarized light source (λ_0 = 632.8 nm) was applied in the LaSFN9 domain. As the incident light wave strikes the array, its power will either be absorbed, reflected, or transmitted through the structure. The absorbed power was computed through the volume integration of the resistive heating in the gold nanoparticles, gold film, and chromium film. The reflected (or transmitted) power was calculated through the surface integration of the far-field power flow at the LaSFN9 (or water) side. The sum of calculated power of absorption, reflection, and transmission is checked against the incident power to ensure the accuracy of simulation.

After solving the three-dimensional Maxwell's equations, we could plot the percentage of power reflected back to the prism and compare it with the experimental measurement. More importantly, we could also plot the percentage of power absorbed in various parts of the structure, for example, in gold nanoparticles and in gold films, to identify the dominant excitation process. Optical power absorbed in gold nanoparticle is relevant to the localized surface plasmon (LSP) excitation in the nanoparticle, whereas power absorbed in gold film is more relevant to the propagating surface plasmons (i.e., cSPR or

DOI: 10.1021/acs.analchem.6b03798
Anal. Chem. 2016, 88, 11924−11930

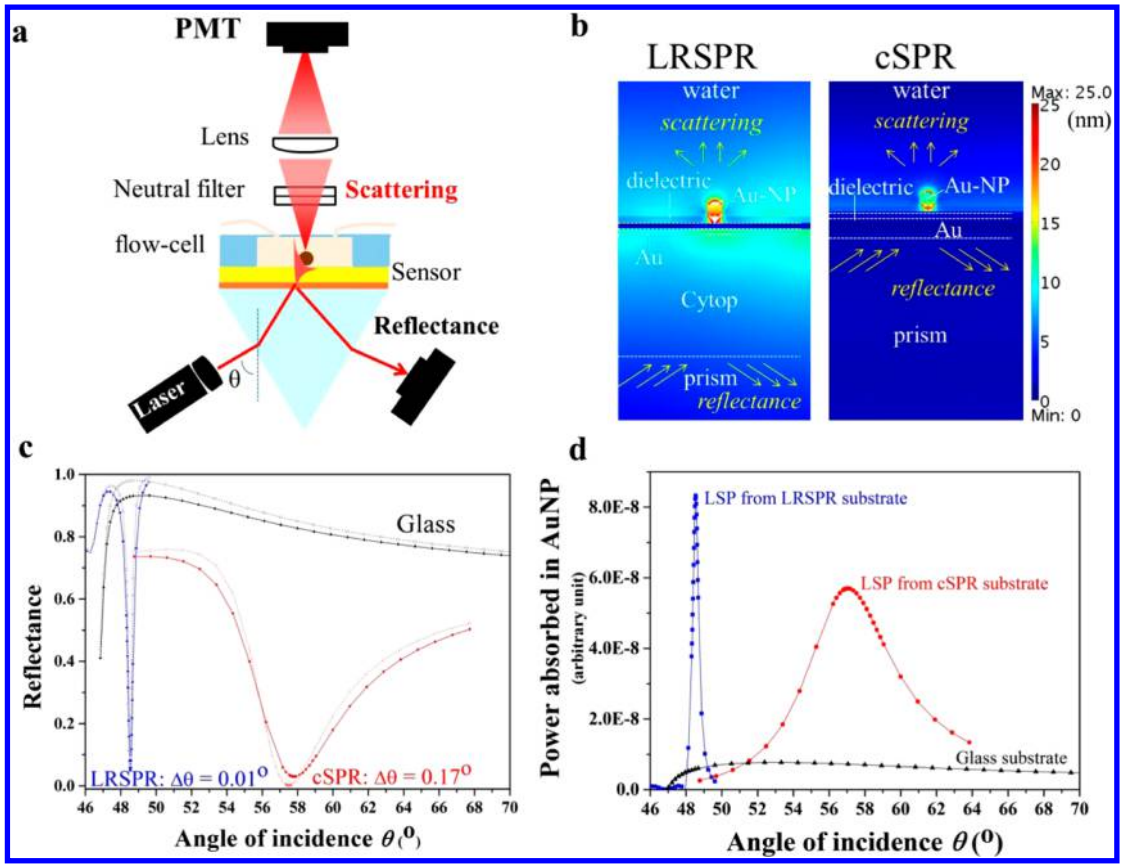

Figure 1. (a) Schematic illustration of the optical setup for SPR refractometric and scattering measurements. (b) Simulated field distribution on the cross-section of LRSPR and cSPR chips attached with 36 nm AuNPs with 15 nm away from the sensor surface and interparticle distance of 500 nm. Simulated (c) angular reflectivity spectra and (d) angular scattering spectra for the LRSPR and cSPR sensor chip attached with AuNPs corresponding to (b).

LRSPR in this context). By doing these extra analyses from simulations, we may discover the true physics/mechanism behind the experimental observation on power reflection. In addition, the near field information at the resonant incident angle in which we are more interested can be directly obtained from the simulations as well. A dielectric thickness (denoted as the distance between the AuNPs and the sensor surface) of 15 nm and a pitch (denoted as the average distance between AuNPs) of 500 nm were used in the simulations. The 15 nm spacing was chosen here on the basis of the approximated distance between the Au film and AuNP tags for the cTnI probe/target used in the experimental study.

RESULTS AND DISCUSSION

The schematic illustrations of the optical setup for SPR measurements and the geometries employed in the simulations are shown in Figure 1a,b. Two measurement schemes (i.e., conventional refractometric scheme vs SP-LS scheme) and three substrates (i.e., glass, SPR supported chip and LRSPR supported substrates) are studied. Long-range surface plasmon resonance (LRSPR) has emerged as a promising alternative to conventional SPR (cSPR) biosensing[11,27,28] as it offers up to 8-fold enhancement of penetration depth into the sensing medium and 20-fold improved figure-of-merit, due to the inherently larger enhancement of the intensities of electromagnetic fields associated with long-range surface plasmons in comparison to conventional surface plasmons.[29,30] We therefore systematically investigated in this study the application of the SP-LS to both cSPR and LRSPR.

In conventional refractometric measurement SPR sensing schemes, the binding of AuNPs resulting from molecular recognition to the biological target is used to amplify the SPR signal that is collected by the reflectance detector (Figure 1a). On the other hand, in the SP-LS measurement scheme, the scattered light emitted at the sensor surface passes through a quartz window, a neutral filter, and is collected by the photomultiplier tube (PMT). At the resonant angle, surface plasmons are excited, resulting in a reflection dip, an absorption peak, and a transmission peak. Due to the excitation of the propagating plasmons at the water/gold interface, more optical power is transmitted to the water side (also the AuNP side) of the sensor. It is this amount of transmitted optical power that is seen and scattered by the AuNPs. Figure 1b clearly shows this effect. AuNPs with a diameter of ~36 nm were synthesized and used in both refractometric and SP-LS experiments. Results from AuNPs adsorption on three different substrates (i.e., glass, SPR supported chip and LRSPR supported substrate) were compared in terms of the refractometric (Figure 1c) and scattering changes (Figure 1d). In the simulated result shown in Figure 1c, the adsorption of AuNPs on cSPR sensor induced a large angular shift as compared with that of LRSPR, suggesting that cSPR is more sensitive to the presence of AuNPs than LRSPR in the refractometric scheme.[31] As expected, no resonant angle was detected on the glass substrate even if coated with AuNPs. Next, the scattered intensities from these

DOI: 10.1021/acs.analchem.6b03798
Anal. Chem. 2016, 88, 11924−11930

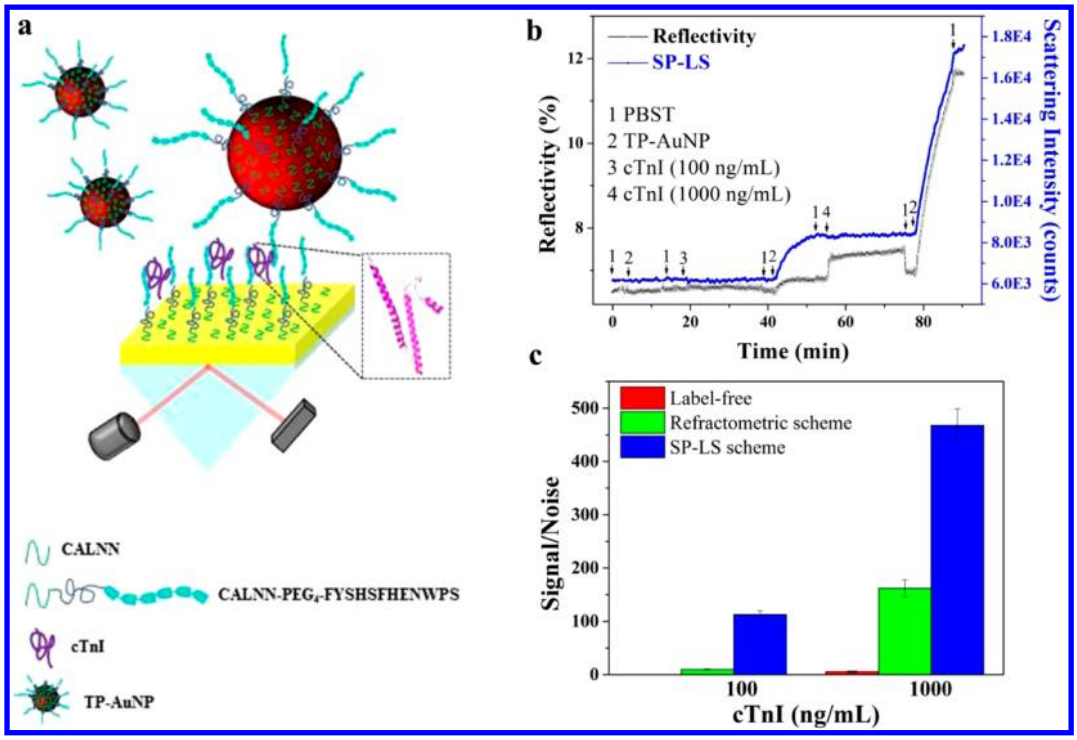

Figure 2. (a) Schematic illustration of the sandwich assay used for the SP-LS detection of troponin. (b) Kinetic data for cTnI detection based on cSPR sensor. (c) Comparison of sensitivities of the cSPR refractometric and scattering enhancement schemes.

substrates were simulated, as shown in Figure 1d. This study shows that LRSPR provides higher maximal scattering intensity of AuNPs than that of cSPR. This is ascribed to the higher electromagnetic field on the surface of LRSPR chip as compared with cSPR, as shown in Figure 1b. This result suggests that LRSPR provides higher sensitivity for the measurement of AuNPs scattering than cSPR. Interestingly, the scattering intensity from AuNPs-coated bare glass substrate was about 10-fold weaker than SPR schemes indicating that the AuNPs without coupling of the surface plasmon contribute minimally to scattering, which is in good agreement with previous findings.[24]

In order to investigate the relevance of the proposed SP-LS strategy as an amplification scheme for biosensing, a biomolecular sandwich assay for the detection of cTnI was experimentally employed, as shown in Figure 2a. To this end, AuNPs with diameters of ∼36 nm were synthesized and functionalized with a peptide binder TP (CALNN-Peg4-FYSHSFHENWPS, specific to cTnI) and a peptide spacer (CALNN) at the molar ratio of 1 to 1, as described in the Experimental Section. The UV−vis measurement (Figure S1c) confirmed that no aggregation took place during the modification of the AuNPs, which is important as the scattering properties are strongly influenced by the size and aggregation state of the AuNPs.

Next, a planar SPR Au sensor chip was functionalized with the TP peptide binder and mounted in the SPR setup. The TP-functionalized AuNPs (TP-AuNPs) are used as an amplifier on the sandwich assay as depicted in Figure 2a. Kinetic measurements for conventional SPR were obtained by fixing the incident angle at θ = 56.8° (Figure 2b), which is the location with the highest reflectivity−angular slope ($\partial R/\partial\theta$) at the edge of the cSPR reflectivity curve. In a typical experiment, the TP-biofunctionalized SPR sensor surface was rinsed with PBST (PBS buffer with 0.05% Tween-20) for 2 min to obtain a stable baseline. To investigate the nonspecific adsorption of the TP-AuNPs on the sensor chip, 0.1 nM of TP-AuNPs solution was first flowed over the sensor surface for 10 min, followed by rinsing with PBST for 3 min. As shown in Figure 2b, no changes in the baseline were observed for both the refractometric and scattering measurements, demonstrating that the nonspecific adsorption of TP-AuNPs was well below the noise level. Next, two concentrations (100 and 1000 ng/mL) of cTnI in PBST were injected into the flow-cell separately and circulated for 20 min.

After a short wash with PBST for 3 min, the 0.1 nM TP-AuNPs solution was then injected to form a sandwich assay. The refractometric and scattering schemes were simultaneously monitored. As shown in Figure 2b, the measured changes in reflectivity and scattering intensities amplified by TP-AuNPs at 100 ng/mL cTnI were 0.26% and 2075 counts, respectively. The signal-to-noise ratio (SNR) was employed to compare the two amplification schemes, as shown in Figure 2c. The scattering scheme provided 12-fold and 2.9-fold higher SNR than the AuNPs-enhanced refractometric scheme at the two tested cTnI concentrations. Note that there was negligible change in reflectivity in response to cTnI binding in the label-free experiment at 100 ng/mL, and a small reflectivity change of ∼0.25% for 1000 ng/mL cTnI. Under these experimental conditions, the SNR of label-free response for refractometric measurement is about 85-fold lower than that obtained with the SP-LS measurement, as shown in Figure 2c. These experimental results indicate that SP-LS provide higher sensitivity than refractometric scheme especially for the detection of low quantity of AuNPs on the sensors surface.

To further determine the potential of the SP-LS sensing approach and better understand the correlation between the surface coverage of AuNPs and scattered light intensity, a systematic study employing both cSPR and LRSPR was conducted on a model sandwich assay of cTnI (Figure 2a).

DOI: 10.1021/acs.analchem.6b03798
Anal. Chem. 2016, 88, 11924−11930

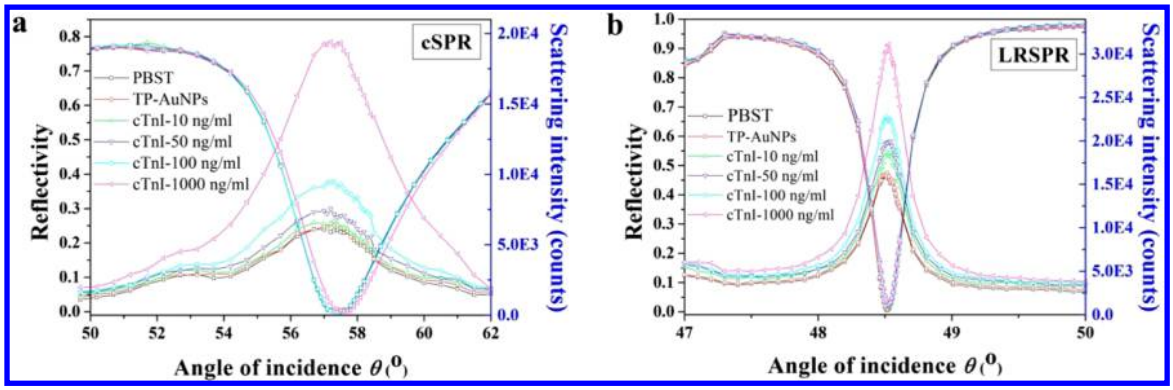

Figure 3. Angular reflectivity and scattering spectra as a function of cTnI concentrations for (a) cSPR and (b) LRSPR.

To this end, TP-functionalized sensing surfaces were exposed to cTnI (10, 50, 100, 1000 ng/mL) in PBST and subsequently incubated with 0.1 nM TP-AuNPs for 10 min. The reflectivity and scattering intensity changes were recorded for both cSPR (Figure 3a) and LRSPR (Figure 3b). The AuNPs-enhanced refractometric measurements show negligible changes of the resonant angle for cTnI concentrations lower than 100 ng/mL.

At cTnI = 1000 ng/mL, the resonant angle shifts 0.2° and ~0.01° for cSPR and LRSPR, respectively. The results are consistent with the simulations shown in Figure 1c, demonstrating that cSPR is more sensitive than LRSPR for AuNPs-enhanced refractometric measurement. As compared with the angular reflectivity, the scattering spectra for both cSPR and LRSPR show a significant increase in the scattering intensity with an increased concentration of cTnI. The results are summarized in Figure 4a to allow for a direct comparison of the two amplification schemes. In the AuNPs-enhanced refractometric scheme, there was no significant response for cTnI concentrations of less than 100 ng/mL for both cSPR and LRSPR (see an example of cSPR for 50 ng/mL cTnI in the Supporting Information, Figure S2). However, in the SP-LS measurement, both cSPR and LRSPR show detectable scattering intensity changes for the detection of 10 ng/mL cTnI. In addition, LRSP-LS demonstrates a higher response as compared to cSP-LS at cTnI concentration lower than 100 ng/mL, suggesting that LRSP-LS is more sensitive at low surface coverage of AuNPs. This observation is confirmed by calculation of the limit of detection (LOD) for cSPR and LRSPR extrapolated from Figure 4a. LODs were determined as the intersection of the calibration curve with 3 times the standard deviation of the scattering signal baseline (dashed blue line). A LOD of 0.2 ng/mL was achieved for LRSP-LS that was 10-fold lower than that for cSP-LS determined to be 2 ng/mL. Although only two data points were available for cSPR and LRSPR in the AuNPs-enhanced refractometric mode, LODs were estimated to be in the order of 35 ng/mL and 20 ng/mL, respectively. These results demonstrate the superiority of the SP-LS approach over the refractometric one.

Finally, a simulation was carried out using the finite element method to provide a physical insight into the effect of AuNPs density/pitches (interparticle distance) to the SP-LS scheme and elucidate the observed differences between cSPR and LRSPR. Note that the size and shape of the AuNP tags used in the study were not highly monodisperse, and this might have contributed in part to the observed discrepancy between the theoretical results and experimental data. In the simulation, five different pitches (interparticle distance of 150, 200, 400, 500, and 800 nm were used for theoretical investigation, as shown in Figure 4. First, Figure 4b shows the absorption intensity of AuNPs on cSPR and LRSPR substrates. As expected, the absorption intensity of AuNPs increased with increasing AuNPs density (i.e., decreased interparticle distance) both for cSPR and LRSPR sensor substrates. However, at pitches $p > 200$ nm (i.e., low density of particles), the simulation reveals that LRSPR provides higher absorption intensity, as compared with cSPR, whereas for higher surface coverage ($p < 150$ nm), cSPR offers higher absorption intensity. Here the calculated absorption intensity in AuNPs (instead of scattering intensity) is used for the theoretical analysis because it provides more direct information on excitation of AuNPs plasmons, whereas scattering intensity contains both information on AuNPs plasmon and propagating plasmons. To obtain further insights into the physical mechanisms, absorption intensity in AuNPs should be used[32] (more details can be found in simulations in ref 28).

This absorption intensity (Figure 4b) is directly relevant to the total electric field enhancement (FE) $|E/E_0|$ induced per AuNPs (Figure 4c,d). Together, they can be used to explain the experimental finding presented in Figure 4a. As shown in Figure 4c for the case of cSPR and Figure 4d for LRSPR, LRSPR provides higher FE (similarly, higher absorption intensity in AuNPs as in Figure 4b) than cSPR at large pitches (less particles). For instance, at $p = 800$ nm, LRSPR exhibits 2-fold higher FE than that of cSPR, which is consistent with the higher scattering for LRSPR than cSPR in Figure 4a. On the other hand, at high particle density (e.g., $p = 150$ nm), the FE per AuNPs is higher for cSPR, and the scattering intensity for cSPR at $p = 150$ nm is consistently higher than that of LRSPR (Figure 4a). Therefore, the electric field enhancement on SPR sensor surface is crucial for the scattering intensity of the AuNPs. This is similar to surface-plasmon-enhanced fluorescence spectroscopy (SPFS),[33,34] as the scattering intensity of the AuNPs is increased by the high electric field enhancement associated with the high input of power absorbed by the nanoparticles.

Simulations of the angular spectra were next performed to further understand this point presented in Figure 4e. There is only a small damping of the SPs when the pitch decreases from 800 to 500 nm for both LRSPR and cSPR. However, once the pitch is smaller than 200 nm, the SP damping is more severe for the case of LRSPR than that of cSPR as shown by the minimal reflectivity increase (Figure 4e). As the propagating SPs are damped, the field around the propagating interface of the Au film and AuNPs is weakened, which results in a decrease of the

DOI: 10.1021/acs.analchem.6b03798
Anal. Chem. 2016, 88, 11924−11930

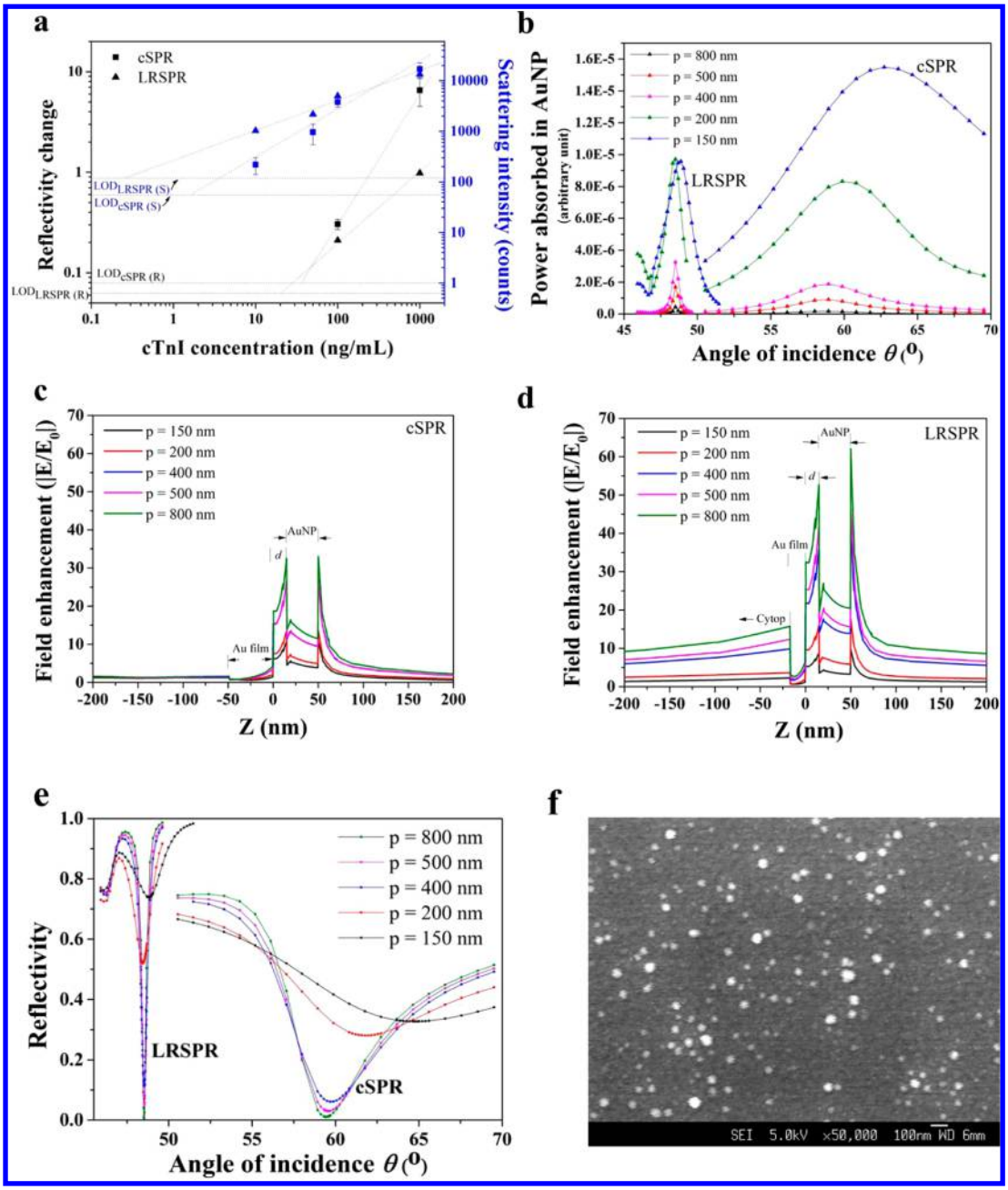

Figure 4. (a) Calibration curves for the detection of cTnI by AuNPs-enhanced refractometric cSPR (black square), cSP-LS (blue square), AuNPs-enhanced refractometric LRSPR (black triangle), and LRSP-LS (blue triangle). (b) Simulated angular adsorption of AuNPs with various pitches on cSP-LS and LRSP-LS. The cross-section of electric field amplitude $|E/E_0|$ as a function of z from the surface for (c) cSPR and (d) LRSPR sensor chip modified with 36 nm AuNPs at different pitches. (e) Simulated angular spectra vs AuNPs pitches for 36 nm AuNPs at-tached on cSPR and LRSPR substrate. (f) SEM image of a SPR sensor chip attached with AuNPs after sandwich assay of 1000 ng/mL cTnI, indicating an average pitch of p = 415 nm.

field enhancement. In summary, at low AuNPs densities (800 nm < p < 500 nm), the higher electromagnetic field associated with LRSPR in comparison to that of cSPR results in higher scattering intensities. However, at higher AuNPs densities (p < 200 nm), the significant damping of LRSP translates into decreased field enhancement, which leads to lower scattering intensity for LRSPR in comparison to cSPR.

To further corroborate the simulation obtained using the finite element method to the experimental data, SEM measurements were carried out to determine the AuNPs interparticle distance associated with the concentration of 1000 ng/mL cTnI. Analysis of the SEM images indicated that the average interparticle distance is ~415 nm for this specific experimental condition (Figure 4f). At such a pitch, cSPR is theoretically predicted to provide comparable scattering intensity than LRSPR (Figure 4b), in agreement with the experimental SP-LS data.

CONCLUSIONS

In conclusion, surface-plasmon-enhanced light scattering of nanoparticle secondary probes has been used for the first time as an amplification scheme for biosensing applications. Both simulation and experimental studies confirmed the significant signal amplification resulting from SP-LS. Experimental results

DOI: 10.1021/acs.analchem.6b03798
Anal. Chem. 2016, 88, 11924−11930

using AuNPs-enhanced cTnI assay demonstrated that SP-LS provides up to 2 orders of magnitude higher sensitivity than conventional refractometric schemes for both conventional surface plasmon resonance and long-range surface plasmon resonance substrates. In addition, a 10-fold LOD improvement was achieved for the detection of cTnI based on LRSPR SP-LS as compared with cSPR. Theoretical studies show that the improved LOD is due to the inherently higher field intensity for LRSPR at low AuNPs densities. Further studies to determine the structure function relationship of the AuNPs in SP-LS biosensing are warranted to further optimize this new biosensing concept. Considering the excellent results obtained in this study, we expect that surface-plasmon-enhanced light scattering will be employed in the near future as a highly sensitive method for immune-sandwich biosensing applications.

■ ASSOCIATED CONTENT

Supporting Information

The Supporting Information is available free of charge on the ACS Publications website at DOI: 10.1021/acs.analchem.6b03798.

DLS and TEM characterization, UV−vis spectra, time-dependent reflectivity data, description for calculation of refractive index unit (PDF)

■ AUTHOR INFORMATION

Corresponding Authors

*E-mail: Benjamin.thierry@unisa.edu.au. Tel.: +61 8 83023689. Fax: + 61 8 8302 3683.
*E-mail: wangyi@wibe.ac.cn.
*E-mail: bliedberg@ntu.edu.sg.

ORCID

Benjamin Thierry: 0000-0002-6757-2842

Notes

The authors declare no competing financial interest.

■ ACKNOWLEDGMENTS

This project is supported by the National Health and Medical Research Council of Australia and Wenzhou government's startup grant (WIBEZD2014004-02). This work was performed (in part) at the South Australian node of the Australian National Fabrication Facility under the National Collaborative Research Infrastructure Strategy to provide nano and micro-fabrication facilities for Australia's researchers. The authors would like to thank Dr. Yu-Ming Yang for his help on the calculations of interparticle distances of AuNPs for SEM images. B.L. and W.Y. acknowledge support from Ministry of Education, Singapore, through MOE-2014-T1001-133, and from the Provostäs Office, NTU, Singapore.

■ REFERENCES

(1) Brolo, A. G. *Nat. Photonics* **2012**, *6*, 709−713.
(2) Lee, K. L.; Chih, M. J.; Shi, X.; Ueno, K.; Misawa, H.; Wei, P. K. *Adv. Mater.* **2012**, *24*, OP253−OP259.
(3) Zijlstra, P.; Paulo, P. M.; Orrit, M. *Nat. Nanotechnol.* **2012**, *7*, 379−382.
(4) Guo, L.; Jackman, J. A.; Yang, H.-H.; Chen, P.; Cho, N.-J.; Kim, D.-H. *Nano Today* **2015**, *10*, 213−239.
(5) Lee, H. J.; Li, Y.; Wark, A. W.; Corn, R. M. *Anal. Chem.* **2005**, *77*, 5096−5100.
(6) Li, Y.; Lee, H. J.; Corn, R. M. *Anal. Chem.* **2007**, *79*, 1082−1088.
(7) Sendroiu, I. E.; Gifford, L. K.; Lupták, A.; Corn, R. M. *J. Am. Chem. Soc.* **2011**, *133*, 4271−4273.
(8) Wang, Y.; Dostalek, J.; Knoll, W. *Anal. Chem.* **2011**, *83*, 6202−6207.
(9) Zeng, S.; Baillargeat, D.; Ho, H.-P.; Yong, K.-T. *Chem. Soc. Rev.* **2014**, *43*, 3426−3452.
(10) Yu, F.; Persson, B.; Löfås, S.; Knoll, W. *J. Am. Chem. Soc.* **2004**, *126*, 8902−8903.
(11) Wang, Y.; Brunsen, A.; Jonas, U.; Dostalek, J.; Knoll, W. *Anal. Chem.* **2009**, *81*, 9625−9632.
(12) He, L.; Musick, M. D.; Nicewarner, S. R.; Salinas, F. G.; Benkovic, S. J.; Natan, M. J.; Keating, C. D. *J. Am. Chem. Soc.* **2000**, *122*, 9071−9077.
(13) Liu, T.; Thierry, B. *Langmuir* **2012**, *28*, 15634−15642.
(14) Maurer, T.; Adam, P.-M.; Lévêque, G. *Nanophotonics* **2015**, *4*, 363−382.
(15) Lyon, L. A.; Musick, M. D.; Natan, M. J. *Anal. Chem.* **1998**, *70*, 5177−5183.
(16) Mustafa, D. E.; Yang, T.; Xuan, Z.; Chen, S.; Tu, H.; Zhang, A. *Plasmonics* **2010**, *5*, 221−231.
(17) Hong, X.; Hall, E. A. *Analyst* **2012**, *137*, 4712−4719.
(18) Kwon, M. J.; Lee, J.; Wark, A. W.; Lee, H. J. *Anal. Chem.* **2012**, *84*, 1702−1707.
(19) Špringer, T.; Ermini, M. L.; Špačková, B.; Jabloňků, J.; Homola, J. *Anal. Chem.* **2014**, *86*, 10350−10356.
(20) Law, W.-C.; Yong, K.-T.; Baev, A.; Prasad, P. N. *ACS Nano* **2011**, *5*, 4858−4864.
(21) Storhoff, J. J.; Lucas, A. D.; Garimella, V.; Bao, Y. P.; Müller, U. R. *Nat. Biotechnol.* **2004**, *22*, 883−887.
(22) El-Sayed, I. H.; Huang, X.; El-Sayed, M. A. *Nano Lett.* **2005**, *5*, 829−834.
(23) Ciracì, C.; Hill, R.; Mock, J.; Urzhumov, Y.; Fernández-Domínguez, A.; Maier, S.; Pendry, J.; Chilkoti, A.; Smith, D. *Science* **2012**, *337*, 1072−1074.
(24) Jory, M.; Cann, P.; Sambles, J. R.; Perkins, E. *Appl. Phys. Lett.* **2003**, *83*, 3006−3008.
(25) Agnarsson, B.; Lundgren, A.; Gunnarsson, A.; Rabe, M.; Kunze, A.; Mapar, M.; Simonsson, L.; Bally, M.; Zhdanov, V. P.; Höök, F. *ACS Nano* **2015**, *9*, 11849−11862.
(26) Frens, G. *Nature, Phys. Sci.* **1973**, *241*, 20−22.
(27) Méjard, R.; Griesser, H. J.; Thierry, B. *TrAC, Trends Anal. Chem.* **2014**, *53*, 178−186.
(28) Krupin, O.; Asiri, H.; Wang, C.; Tait, R. N.; Berini, P. *Opt. Express* **2013**, *21*, 698−709.
(29) Huang, C. J.; Dostalek, J.; Knoll, W. *J. Vac. Sci. Technol. B* **2010**, *28*, 66−72.
(30) Brigo, L.; Gazzola, E.; Cittadini, M.; Zilio, P.; Zacco, G.; Romanato, F.; Martucci, A.; Guglielmi, M.; Brusatin, G. *Nanotechnology* **2013**, *24*, 155502.
(31) Yang, C.-T.; Wu, L.; Bai, P.; Thierry, B. *J. Mater. Chem. C* **2016**, *4*, 9897−9904.
(32) Wu, L.; Bai, P.; Li, E. P. *J. Opt. Soc. Am. B* **2012**, *29*, 521−528.
(33) Dostálek, J.; Kasry, A.; Knoll, W. *Plasmonics* **2007**, *2*, 97−106.
(34) Wang, Y.; Dostálek, J.; Knoll, W. *Biosens. Bioelectron.* **2009**, *24*, 2264−2267.

DOI: 10.1021/acs.analchem.6b03798
Anal. Chem. 2016, 88, 11924−11930